INTRINSIC ELLIPTICITY CORRELATION OF SDSS LUMINOUS RED GALAXIES AND MISALIGNMENT WITH THEIR HOST DARK MATTER HALOS

TEPPEI OKUMURA[1], Y. P. JING[1], AND CHENG LI[1,2]

[1] Key Laboratory for Research in Galaxies and Cosmology, Shanghai Astronomical Observatory, Chinese Academy of Sciences, 80 Nandan Road, Shanghai, 200030, China; teppei@shao.ac.cn

[2] Max-Planck-Institut für Astrophysik, Karl-Schwarzschild-Strasse 1, 85748 Garching, Germany

ABSTRACT

We investigate the orientation correlation of giant elliptical galaxies by measuring the intrinsic ellipticity correlation function of 83,773 luminous red galaxies (LRGs) at redshifts 0.16–0.47 from the Sloan Digital Sky Survey. We have accurately determined the correlation up to 30 h^{-1} Mpc. Luminosity dependence of the ellipticity correlation is also detected although the error bars are large, while no evidence is found for its redshift evolution between $z = 0.2$ and $z = 0.4$. Then we use a cosmological N-body simulation to examine misalignment between the central LRGs and their parent dark matter halos. Central and satellite galaxies are assigned to simulated halos by employing a halo occupation distribution model for the LRGs. The ellipticity correlation is predicted to have the same shape as, but an amplitude about four times higher than, our observation if the central LRGs are perfectly aligned with their host halos. This indicates that the central LRG galaxies are preferentially but not perfectly aligned with their host halos. With the assumption that there is a misalignment angle between a central LRG and its host halo which follows a Gaussian distribution with a zero mean and a width σ_θ, we obtain a tight constraint on the misalignment parameter, $\sigma_\theta = 35.4^{+4.0}_{-3.3}$ deg. This type of intrinsic ellipticity correlation, if not corrected, can lead to contamination at 5% level to the shear power spectrum in weak lensing surveys of limiting magnitude $R_{AB} = 24.5$ if the source central galaxies follow the same misalignment distribution as the LRGs.

Key words: cosmology: observations – galaxies: elliptical and lenticular, cD – galaxies: formation – galaxies: halos – large-scale structure of universe – methods: statistical

Online-only material: color figures

1. INTRODUCTION

Weak gravitational lensing by large-scale structure provides a unique tool that directly probes matter distribution in the universe. One of the most serious sources of contamination for weak lensing observations comes from two types of intrinsic alignments: the ellipticity correlation of source galaxies with each other (intrinsic ellipticity–intrinsic ellipticity correlation) and the ellipticity correlation of source galaxies with the surrounding matter distribution (gravitational shear–intrinsic ellipticity correlation).

There was much work based on both analytical and numerical methods which attempted to estimate the intrinsic ellipticity–intrinsic ellipticity correlation (Heavens et al. 2000; Croft & Metzler 2000; Lee & Pen 2000, 2001; Catelan et al. 2001; Crittenden et al. 2001; Jing 2002). According to these previous studies, the effect of intrinsic alignment can lead to $\sim 10\%$ or even higher contamination for a deep survey with median source redshift of 1 if galaxies are aligned with the angular momentum or the ellipticity of their host halos. Fortunately, this effect can be reduced by downweighting nearby source pairs with either spectroscopic or photometric redshifts (King & Schneider 2002; Heymans & Heavens 2003; Takada & White 2004; King 2005; Fan 2007). Although the intrinsic ellipticity–intrinsic ellipticity correlation has been detected in several observations at low redshift (Pen et al. 2000; Bernstein & Norberg 2002; Brown et al. 2002; Hirata et al. 2004; Heymans et al. 2004; Lee & Pen 2007), the amplitude of the correlation is much smaller than theoretical predictions (Heymans et al. 2004; Mandelbaum et al. 2006b; Heymans et al. 2006), which indicates that galaxies are not perfectly aligned with the angular momentum or the ellipticity of

their host halos. Heymans et al. (2004) explained the discrepancy in amplitude of the ellipticity correlation function between the model predictions and the observations by assigning a random misalignment angle around the original halo angular momentum vector. On the other hand, Hoekstra et al. (2004) detected the significant flattening of dark matter halos along the minor axes of galaxies from weak lensing analysis, which implies that the halos are well aligned with the major axes of the galaxies. In a later work, however, Mandelbaum et al. (2006a) did not detect this effect even using a much larger SDSS data set.

There are also observational studies which have detected with a high confidence the gravitational shear–intrinsic ellipticity correlation (Mandelbaum et al. 2006b; Hirata et al. 2007), although downweighting this effect is more complicated (Hui & Zhang 2008; Hirata & Seljak 2004; Heymans et al. 2006; Bridle & King 2007; Joachimi & Schneider 2008). In this paper, we focus only on the intrinsic ellipticity–intrinsic ellipticity correlation, so we call it the intrinsic ellipticity correlation for brevity.

Meanwhile, investigating intrinsic alignment of galaxies relative to their host halos is also important because it contains information about galaxy formation and evolution. Recently there has been increasing interest in the misalignment between central galaxies and their parent dark matter halos. It was shown in previous studies based on N-body simulations that the angular momentum distributions of gas and dark matter components are partially aligned, with a typical misalignment angle of $\sim 30°$ (van den Bosch et al. 2002; Chen et al. 2003; Sharma & Steinmetz 2005), but this might be relevant to disk galaxies only. It is also expected that the central ellipticals are aligned with their host halos to a certain degree if the ellipticals are formed by

dry mergers (Dubinski 1998; Naab et al. 2006; Boylan-Kolchin et al. 2006), because the orientations of the central ellipticals and of the host dark matter halos are respectively determined by the orbital angular momenta of their progenitor galaxies and halos that are correlated. In observation, by studying the alignment of central galaxies with their satellite spatial distributions in SDSS groups (Yang et al. 2006) and by assuming that the satellites follow dark matter in spatial distribution, Kang et al. (2007) and Wang et al. (2008) have reached somewhat conflicting conclusions about the misalignment angle between the central galaxies and their host halos (typically $40°$ in Kang et al. (2007) and $23°$ in Wang et al. (2008)).

In this paper, we present the ellipticity correlation functions of a spectroscopic luminous red galaxy (LRG) sample from the Sloan Digital Sky Survey (SDSS; York et al. 2000). We estimate the luminosity and redshift dependences of the ellipticity correlations. LRGs are massive, and most of them are located in the central regions of rich groups or galaxy clusters. A small fraction of satellites can be reliably identified in the observation. Therefore, we are able to study the misalignment between central LRGs and their parent dark halos by comparing the observed ellipticity correlation function with that of the dark halos in an N-body simulation.

Compared to previous work concerning the misalignment, our analysis using the LRG sample have at least three advantages. First, the orientation of satellite galaxies relative to their host halos might be very different from that of the central galaxies. Central LRGs are easy to identify, which enables us to reliably determine the misalignment of central galaxies with their host halos without contamination from satellite galaxies. Second, all LRG galaxies are believed to be the product of dry mergers, and their formation processes are distinct from those of spiral (disk) galaxies. Our analysis will be on central ellipticals without contamination from disk galaxies. Finally, because LRGs preferentially reside in massive halos and such host halos have stronger ellipticity correlations than less massive ones hosting fainter galaxies (Jing 2002), it is easier to accurately measure their ellipticity correlations and determine their misalignment angle relative to their host halos.

The structure of this paper is as follows. In Section 2, we describe the SDSS LRG sample used in our analyses. We measure the ellipticity correlation functions of SDSS LRGs in Section 3. The luminosity and redshift dependences of the ellipticity correlation function are also presented. In Section 4, we calculate the model ellipticity correlation functions of LRGs using an N-body simulation with the assumption that central LRGs are completely aligned with their parent dark matter halos. We examine and constrain the misalignment between central LRGs and their parent halos in Section 5. Our conclusions are given in Section 6.

2. SDSS LUMINOUS RED GALAXY SAMPLE

We analyze the LRG sample from the SDSS (York et al. 2000; Stoughton et al. 2002). The LRG selection algorithm (Eisenstein et al. 2001) selects ~ 12 galaxies per square degree using color and magnitude cuts. The resulting galaxies have a Petrosian magnitude $r < 19.5$, which tend to be luminous early-types and to be located in rich groups or clusters of galaxies. All fluxes are corrected for reddening (Schlegel et al. 1998) before use. The LRG selection is so efficient that it produces a volume-limited sample, and thus the comoving number density of the sample is close to a constant out to $z \sim 0.36$ and drops thereafter due to the flux limits (see Figure 1 of Zehavi et al. 2005).
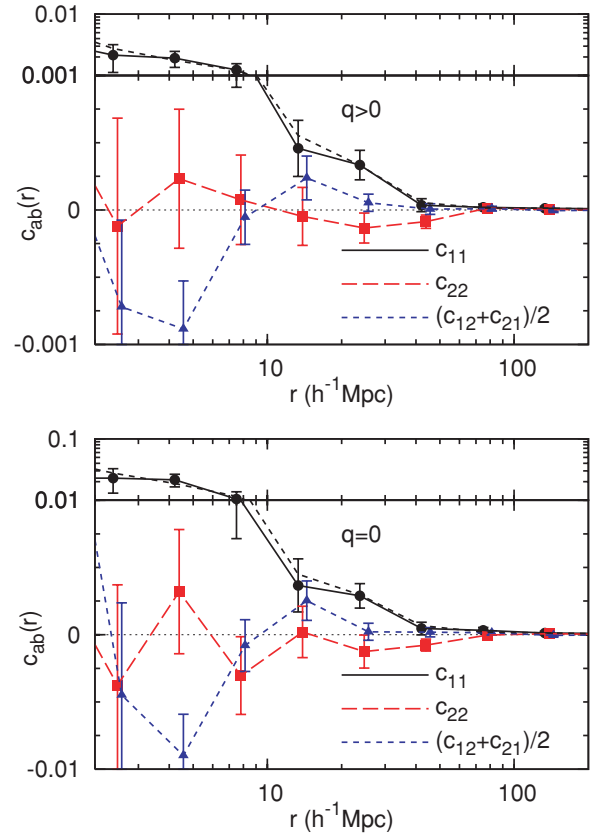

Figure 1. Top: ellipticity correlation functions for the central LRG sample. Bottom: as the top panel, but setting $q = 0$ when the ellipticity of the LRGs is measured in Equation (1). The dashed black line shows c_{11} for the combined sample of central and satellite LRGs. To clearly show the fluctuations of c_{22} and $(c_{12} + c_{21})/2$, mixed logarithmic and linear scalings are used for the vertical axis. Bins in r are in logarithmic separation of 0.25. The circles/triangles have been respectively offset in the negative/positive direction for clarity.

(A color version of this figure is available in the online journal.)

For our analysis we use 83,773 LRGs in the redshift range from 0.16 to 0.47 from the SDSS Data Release 6 (Adelman-McCarthy et al. 2008) which is publicly available. We choose only the LRGs for which the redshift confidence parameter is greater than 0.95. The galaxies in the sample have rest-frame g-band absolute magnitudes $-23.2 < M_g < -21.2$ ($H_0 = 100$ km s^{-1} Mpc^{-1}) with $K + E$ corrections of passively evolved galaxies to a fiducial redshift of 0.3 (see Appendix B of Eisenstein et al. 2001).

The goal of this study is to investigate the misalignment of central galaxies and their host dark matter halos. Accurate measurement of redshifts enables us to divide the LRGs in our sample into centrals and satellites. Following Reid & Spergel (2008), we adopt criteria of $r_\perp \leqslant 0.8\,h^{-1}$ Mpc and $r_\parallel \leqslant 20\,h^{-1}$ Mpc for two galaxies to be in the same halo, where $r_\perp$ and $r_\parallel$ are their separations perpendicular and parallel to the line of sight, respectively. The criteria imply that 79,493 LRGs (94.9%) are centrals, which is consistent with the results not only from mock LRGs described in Section 4.2 but also from observational work by Zheng et al. (2008) and Reid & Spergel (2008). For the halos with two or more LRGs, we regard the brightest as the central one and the others as the satellites.

Besides a sample of LRGs, we also need information on their shapes. There are several model-dependent and model-

independent ways in the SDSS data to measure the ellipticity of galaxies (Stoughton et al. 2002). Following the previous work which investigated the central-satellite alignment (e.g., Brainerd 2005; Yang et al. 2006; Faltenbacher et al. 2007), we adopt the latter and define the ellipticity of galaxies with the ellipticity of the 25 mag arcsec^{-2} isophote in the r band. In addition, the point-spread function (PSF) has been corrected when measuring galaxy shapes in the SDSS imaging pipelines (Fischer et al. 2000; Lupton et al. 2001; Stoughton et al. 2002). More accurate schemes for correcting the PSF were adopted in previous work of weak lensing (Hirata et al. 2004; Mandelbaum et al. 2005). However, the original correction for the PSF in the SDSS should be sufficient for the current analysis because only the position angles of LRGs are used in most of our study.

3. ELLIPTICITY CORRELATION OF LRGS

3.1. Measuring the LRG Ellipticity Correlation Functions

The ellipticity correlation is examined by measuring the ellipticity of each galaxy. The two components of the ellipticity are defined as

$$\begin{pmatrix} e_1 \\ e_2 \end{pmatrix} = \frac{1-q^2}{1+q^2} \begin{pmatrix} \cos 2\beta \\ \sin 2\beta \end{pmatrix}, \qquad (1)$$

where q is the ratio of minor and major axes ($0 \leqslant q \leqslant 1$) and β is the position angle of the ellipticity from the north celestial pole to east (Stoughton et al. 2002). Then the ellipticity correlation functions are defined (e.g., Miralda-Escudé 1991; Heavens et al. 2000; Croft & Metzler 2000; Jing 2002) as

$$c_{ab}(r) = \langle e_a(\mathbf{x})e_b(\mathbf{x} + \mathbf{r}) \rangle, \qquad (2)$$

where $\mathbf{r}$ is the three-dimensional vector of separation r joining a pair of galaxies. The comoving distance to every galaxy, $x(z)$, is calculated by assuming a flat universe with $\Omega_m = 1 - \Omega_\Lambda = 0.3$, where Ω_m and Ω_Λ are the mass density parameter and the cosmological constant parameter, respectively. In Equation (2) the components of the ellipticity, e_1 and e_2, are redefined by rotating by an angle between the north pole and the line connecting the two galaxies on the celestial sphere. Thus, the ellipticity component e_1 (e_2) corresponds to the elongation and compression along (at 45° from) the line joining the two galaxies.

The resulting ellipticity correlation functions for the observed central LRGs (see Section 2) are shown in the top panel of Figure 1. For comparison, the result of c_{11} measured from all the LRGs including satellites is also given, which shows that the difference between the results with and without satellites is very small, because the contribution from the satellites is negligible. The error bars shown in the figure represent 1σ errors estimated with the jackknife resampling method. A description of the method is given at the end of this section.

As for the autocorrelation functions, while we clearly detect the positive correlation of ellipticity in c_{11} particularly on scales less than $30\,h^{-1}$ Mpc, the amplitude of c_{22} is found to be much smaller. It is simply because c_{11} is nearly isotropic but c_{22} is very anisotropic (Croft & Metzler 2000; Jing 2002); thus the amplitude of c_{22} is suppressed when averaged over different directions. On the other hand, the cross-correlations c_{12} and c_{21} should vanish on all scales (Heavens et al. 2000; Croft & Metzler 2000; Jing 2002) and our results observationally confirm that $(c_{12} + c_{21})/2$ fluctuates around zero within the measurement errors except for a point at $r \approx 4\,h^{-1}$ Mpc with a 2σ deviation.
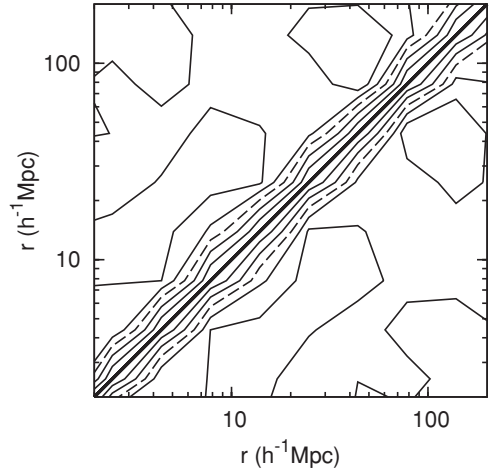

Figure 2. Normalized covariance matrix for the $c_{11}(r)$ measurement of the central LRG sample. Contour spacing is 0.2 going from 1 on the diagonal (thick line) down to 0. The dashed line denotes the 0.4 contour. This is a similar plot to Figure 7 of Zehavi et al. (2005) who focused on the LRG clustering.

In the following analysis the function c_{11} is mainly discussed and c_{22} is used only for a cross-check of the results obtained from the measurement of c_{11}.

The bottom panel of Figure 1 is the same as the top panel, except that it shows the results when the axis ratio q in Equation (1) is set to be zero. It is equivalent to assuming that a galaxy is a line along its major axis, and the measurement indicates the correlation between the orientations of two galaxies with their shape not being considered. This prescription is important because only information on position angles is necessary when we examine the misalignment between LRGs and their parent dark halos. Throughout this paper, we perform all the statistical analyses using the ellipticity correlation functions with $q = 0$. We note that this c_{11} with $q = 0$ is about 10 times larger than that with $q \neq 0$, consistent with the fact that the median value of q is 0.73 for the sample.

Statistical errors on the measurement of the ellipticity correlation functions are estimated using jackknife resampling (e.g., Lupton 1993) with 99 angular subsamples. Because the number of data points used for our statistical analysis is 8, this number of subsamples is large enough to obtain a nonsingular matrix. Each subsample includes a region contiguous on the sky, the comoving size of which is about $120\,h^{-1}$ Mpc on a side at $z = 0.3$.

We obtain the covariance matrix of c_{11} for the central LRGs from the jackknifed realizations by

$$C_{ij} = \frac{N-1}{N} \sum_{l=1}^{N} \left(c_{11}^l(r_i) - \bar{c}_{11}(r_i) \right) \left(c_{11}^l(r_j) - \bar{c}_{11}(r_j) \right), \quad (3)$$

where $N = 99$, $c_{11}^l(r_i)$ represents the value of $c_{11}(r)$ of the ith separation bin in the lth realization, and $\bar{c}_{11}(r_i)$ is the mean value of $c_{11}(r_i)$ over all realizations. Figure 2 shows the obtained covariance matrix normalized by the diagonal elements, $C_{ij}/(C_{ii} \cdot C_{jj})^{1/2}$. As is clearly seen, almost all the contribution of statistical errors comes from the diagonal elements. The error bars shown in Figure 1 are a square root of the diagonals of the matrix, $C_{ii}^{1/2}$. We have tried several values of N, and found that the error bars we obtain are very stable against the changes of N.
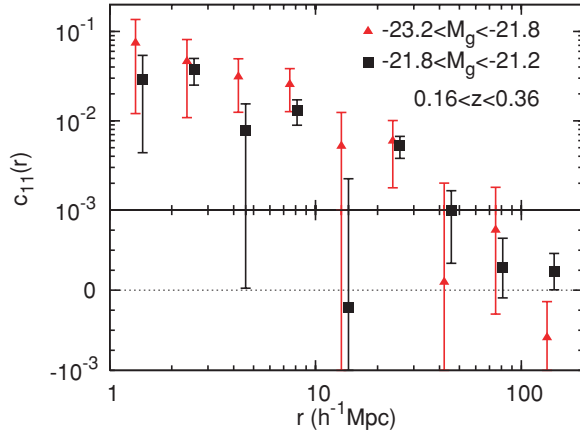
Figure 3. Luminosity dependence of $c_{11}(r)$ of the LRGs for $0.16 < z < 0.36$. Here both the central and satellite LRGs are used for the calculation. Note that the vertical axis mixes logarithmic and linear scalings.

(A color version of this figure is available in the online journal.)
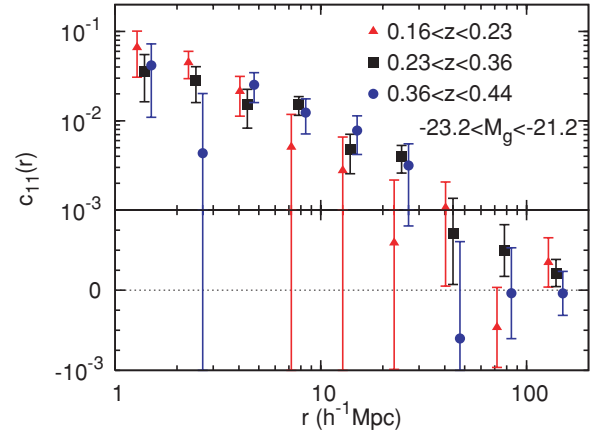

Figure 4. Redshift dependence of $c_{11}(r)$ of the LRGs for the absolute magnitude of $-23.2 < M_g < -21.2$. Here both the central and satellite LRGs are used for the calculation. Note that the vertical axis mixes logarithmic and linear scalings.

(A color version of this figure is available in the online journal.)

3.2. Luminosity and Redshift Dependences

Before proceeding to the next section, we examine the dependences of the measured ellipticity correlation function of LRGs on their luminosity and redshift. Previous studies found a luminosity dependence for the clustering of LRGs (Zehavi et al. 2005; Percival et al. 2007), which indicates that LRGs of different luminosities are in halos of different mass. Because the ellipticity correlation of halos increases with the halo mass (Jing 2002), it is naturally expected that there also exists the luminosity dependence for the ellipticity correlations of galaxies.

Figure 3 shows $c_{11}(r)$ for two spans of M_g at $0.16 < z < 0.36$. The magnitude cuts are similar to those adopted in Zehavi et al. (2005) and the redshift range is chosen to utilize a volume-limited sample. Stronger correlation of ellipticity can be seen in the brighter sample ($-23.2 < M_g < -21.8$) on small scales although the error bars are large because of the sparseness and limited survey volume of the sample. This result is consistent with the expectation that the more luminous LRGs are located in more massive halos (Zehavi et al. 2005; Zheng et al. 2008) that have a stronger ellipticity correlation function (Jing 2002).

Lee & Pen (2008) analyzed simulation data in order to pursue the nonlinear evolution of galaxy intrinsic alignment at $0 < z < 2$. They did not find an indication for the redshift evolution of the ellipticity correlation although they could detect the evolution of its nonlinearity. Thus it may be difficult for current observations to detect the redshift dependence of the ellipticity correlation. Redshift evolution for the LRG clustering was also not detected (Zehavi et al. 2005). Figure 4 shows the redshift dependence of $c_{11}(r)$. Because the redshift range of our LRG sample is not large, even shallower than that examined in Lee & Pen (2008), we do not find such a dependence in the LRG sample.

4. MODEL PREDICTIONS

4.1. N-body Simulation

To make model predictions for the ellipticity correlation function, we use a halo catalog constructed from a high-resolution cosmological simulation with 1024^3 particles in a cubic box of side $1200\,h^{-1}$ Mpc (Jing et al. 2007). A spatially flat ΛCDM model with $\Omega_m = 1 - \Omega_\Lambda = 0.268$, $\Omega_b = 0.045$,

$h = 0.71$, and $\sigma_8 = 0.85$, was assumed, where Ω_b is the baryon density parameter, h is the Hubble parameter normalized by 100 km s^{-1} Mpc^{-1}, and σ_8 is the present linear rms density fluctuation within a sphere of radius $8\,h^{-1}$ Mpc. Dark matter halos are identified in the $z = 0.274$ output using the friends-of-friends algorithm with a linking length b equal to 0.2 times the mean particle separation. See Jing et al. (2007) for details of the simulation.

4.2. Halo Occupation Distribution

In order to assign galaxies to the simulated halos, we rely on the framework of the halo occupation distribution (HOD, e.g., Jing et al. 1998; Ma & Fry 2000; Peacock & Smith 2000; Seljak 2000; Scoccimarro et al. 2001; Berlind & Weinberg 2002), which describes the relationship between the galaxy and dark matter density fields. HOD modeling has been performed for LRG galaxies by several independent approaches (Masjedi et al. 2006; Ho et al. 2007; Blake et al. 2008; Kulkarni et al. 2007; White et al. 2007; Seo et al. 2008; Zheng et al. 2008; Reid & Spergel 2008).

A flexible parameterization with five HOD parameters was introduced by Zheng et al. (2005) (see also Zheng et al. 2007). The mean occupation function of galaxies within a dark halo of mass M, being the sum of central and satellite mean occupation functions, is parameterized as

$$\langle N(M) \rangle = \langle N_{\text{cen}}(M) \rangle \left(1 + \langle N_{\text{sat}}(M) \rangle\right), \qquad (4)$$
$$\langle N_{\text{cen}}(M) \rangle = \frac{1}{2}\left[1 + \text{erf}\left(\frac{\log M - \log M_{\min}}{\sigma_M}\right)\right],$$
$$\langle N_{\text{sat}}(M) \rangle = \left(\frac{M - M_0}{M_1'}\right)^\alpha,$$

where erf is the error function, $M_{\min}$ is the characteristic minimum mass to host a central galaxy, M_1' is a mass for a halo with a central galaxy to host one satellite when $M_0 \ll M_1'$, M_0 is the mass scale to truncate satellites, and σ_M is the characteristic transition width. Following the latest fits for the HOD parameters of the LRGs by Seo et al. (2008), we choose $M_{\min} = 8.226 \times 10^{13}\,M_\odot$, $M_1' = 6.875 \times 10^{14}\,M_\odot$, $M_0 = 3.209 \times 10^9\,M_\odot$, $\sigma_M = 0.556$, and $\alpha = 1.86$. A central LRG is assigned to a halo based on the nearest integer distribution with the average of $\langle N_{\text{cen}}(M) \rangle$. Satellite
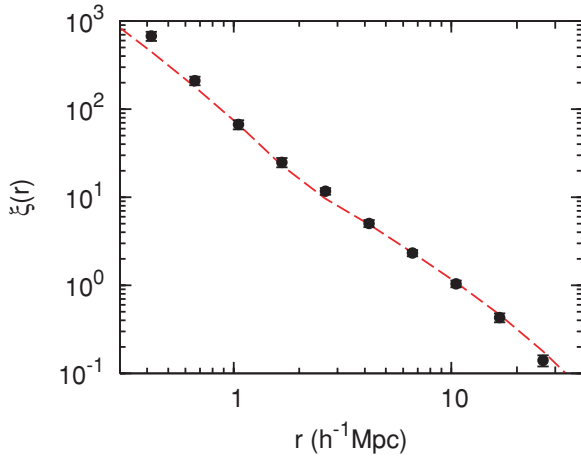
Figure 5. Comparison of the real space correlation functions between the observed and mock LRGs. The black points with the error bars show the observed correlation function (Zehavi et al. 2005). The dashed line is that of the mock galaxy catalog using the best-fit HOD model for the LRGs (Seo et al. 2008).

(A color version of this figure is available in the online journal.)

LRGs are then assigned to each halo with a central based on the Poisson distribution with the average of $\langle N_{\mathrm{sat}}(M) \rangle$. The satellite LRGs inside dark matter halos are distributed following the Navarro–Frenk–White profile (Navarro et al. 1997). The resulting fraction of central LRGs is 93.7%, consistent with that from the observation (Section 2).

In Figure 5, we show a comparison of the real-space correlation function between the mock and observed (Zehavi et al. 2005) LRGs. Very good agreement of the results between the observation and mock catalog can be seen except for $r < 0.5\,h^{-1}$ Mpc, as was seen by Seo et al. (2008). This small discrepancy is irrelevant to the current study because the satellite distribution within halos dominates on this scale and only central LRGs are used for the statistical analysis below.

4.3. Modeled Ellipticity Correlation Function

The principal axes of each halo in a projected plane are computed by diagonalizing the momentum of inertial tensor (e.g., Miralda-Escudé 1991; Croft & Metzler 2000)

$$I_{ij} = \sum x_i x_j, \qquad (5)$$

where the sum is over all the particles in the halo. The ellipticity components of each halo are then estimated in the same way as those of LRGs (Equation (1)), where the value of q is assumed to be zero again.

First, we assume that all central galaxies are completely aligned with their parent dark matter halos. Then the ellipticity correlation functions of central galaxies are equal to those of their parent halos. With this assumption, we plot the ellipticity autocorrelation functions of the mock LRGs, c_{11} and c_{22}, in Figure 6. In order to refine the statistics, we averaged over seven mock LRG samples with different random seeds for assigning LRGs to dark halos. Interestingly, the ellipticity correlation function c_{11} of the mock LRGs has a very similar shape to the observed function, but the amplitude is about four times higher. The function c_{22} is significantly negative at r about a few h^{-1} Mpc, compared to the real observed one. In the next section, we will explain these differences between the observation and
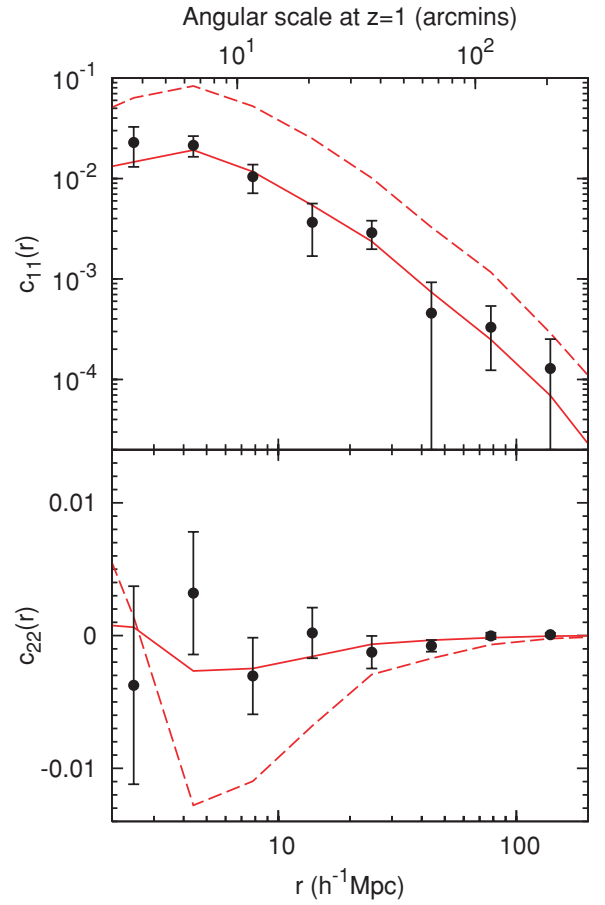

Figure 6. Ellipticity autocorrelation functions of the central LRGs, (top) $c_{11}(r)$ and (bottom) $c_{22}(r)$. In both panels, the data points with the error bars are the measurements from the SDSS, the same ones as those in the bottom panel of Figure 1. The dashed red lines are results of the mock central LRGs with no misalignment with their parent halos. The solid red lines are those with the misalignment parameter of $\sigma_\theta = 35°$. The horizontal axis at the top shows the corresponding angular scale when all the galaxies are located at $z = 1$.

(A color version of this figure is available in the online journal.)

simulation by considering misalignment of central galaxies with their host halos. In Figure 6 we also show the angular separations with the assumption of all the galaxies being at $z = 1$, which is the typical redshift of recent weak lensing surveys (see Section 6). Note that the values of the ellipticity correlation function of halos are about an order of magnitude larger than the previous result by Jing (2002), because we assume $q = 0$ in the current study.

5. CONSTRAINTS ON MISALIGNMENT

In this section we consider a more general case in which the position angle of each central galaxy is not completely aligned with its host halo. We assume that the probability distribution function (PDF) of the misalignment angle θ between the major axes of central LRGs and their host halos is a Gaussian function with a zero mean and a width σ_θ,

$$f(\theta; \sigma_\theta)d\theta = \frac{1}{\sqrt{2\pi}\sigma_\theta} \exp\left[-\frac{1}{2}\left(\frac{\theta}{\sigma_\theta}\right)^2\right]d\theta, \qquad (6)$$

where σ_θ is the misalignment angle parameter or the typical misalignment angle. We artificially assign misalignment to position angles of each mock central LRG according to Equation
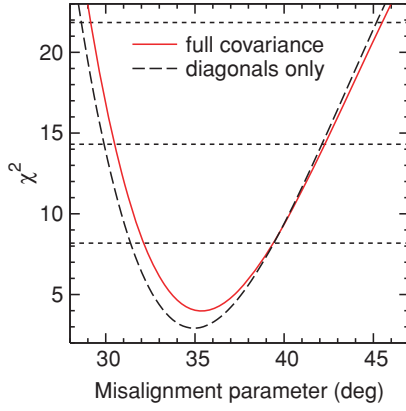
Figure 7. χ^2 distribution for misalignment angle parameter σ_θ. The best-fit parameter is $\sigma_\theta = 35.4^{+4.0}_{-3.3}$ deg (68% C.L.) when we use the full covariance matrix, while $\sigma_\theta = 35.0^{+4.4}_{-3.6}$ deg when we use only the diagonal elements of the covariance. The minimum value of χ^2 is $\chi^2_{min} = 3.983$ and 2.915 with 7 dof, respectively. The horizontal dotted lines show 68%, 95%, and 99% confidence levels.

(A color version of this figure is available in the online journal.)

(6) before the ellipticity correlation function is measured. It is expected that the larger the value of σ_θ is, the smaller the amplitude of the ellipticity correlation function systematically becomes. For each chosen value of σ_θ and each LRG mock sample, we generate nine misaligned LRG samples by choosing different random seeds in order to refine the statistics of our model predictions. Although the obtained nine mock ellipticity catalogs are not independent each other, their average can reduce random fluctuation from different random seeds. Finally, our model prediction for each misalignment parameter σ_θ is calculated by averaging over $7 \times 9 = 63$ misaligned samples.

In comparing the observational data with the model prediction, we first compute the model ellipticity correlation function with a given parameter of σ_θ to be tested. χ^2 statistics are then calculated as

$$\chi^2(\sigma_\theta) = \sum_{i,j} \Delta c_{11}(r_i; \sigma_\theta) C_{ij}^{-1} \Delta c_{11}(r_j; \sigma_\theta), \qquad (7)$$

where C_{ij} is the covariance matrix given by Equation (3), $\Delta c_{11}(r_i; \sigma_\theta)$ the difference between the observed and the model values in the ith separation bin, and i and j run over the number of bins. In this analysis the number of bins is 8 and the degree of freedom is 7. Thus the 99 realizations constructed from jackknife resampling are large enough to derive a nonsingular matrix, as was already stated in Section 3.1. The range of σ_θ in our calculation of χ^2 is $20 < \sigma_\theta < 50°$ with the width of $\Delta\sigma_\theta = 1°$. The binned values of χ^2 are then cubic-spline interpolated.

Figure 7 shows χ^2 as a function of the misalignment parameter σ_θ. For comparison, both the results that all the elements and only diagonals of the covariance matrix are used are given. These two results are in very good agreement, indicating that the non-diagonal elements of the error matrix are not important. The fits of the observed ellipticity correlation function to the model prediction using the full covariances give $\sigma_\theta = 35.4^{+4.0}_{-3.3}$ (68% confidence level), and $\chi^2_{min} = 3.983$ with 7 dof.

The model prediction of c_{11} with $\sigma_\theta = 35°$ is shown in the top panel of Figure 6. As a cross-check, we also plot the model of c_{22} with the same σ_θ in the bottom panel of Figure 6, which is also in very good agreement with the observed c_{22}. This accordance additionally enhances the validity of our analysis.

Recently there were two papers by Kang et al. (2007) and Wang et al. (2008) who studied the misalignment angle between galaxies and their host halos. Although they used the same observed statistics of the alignment angle between the major axis of the central galaxies and their connecting lines to satellites (Yang et al. 2006), they obtained the typical misalignment angle with different results (about 40° by Kang et al. (2007) and 23° by Wang et al. (2008) for the whole sample of blue and red central galaxies in their papers). The difference may come from their different methods to trace the satellite spatial distribution in their modeling. Kang et al. (2007) have used a semi-analytical model to trace satellites, and Wang et al. (2008) have first tried to determine the spatial distribution of satellites within halos. The discrepancy might come from the fact that the triaxial shape of satellite distribution within groups determined by Wang et al. (2008) is much rounder than dark matter halos in simulations (Jing & Suto 2002; Kang et al. 2007). Our analysis does not need to make any assumption for the satellite galaxies or the shape of halos. Because LRGs are red centrals, our results should be compared with the misalignment value 16.6 ± 0.1 degrees for red centrals in Wang et al. (2008)(their Table 2). Their value is significantly smaller than ours, and such a small value is strongly rejected by our analysis.

6. CONCLUSIONS

We have measured the ellipticity auto- and cross-correlation functions $c_{ab}(r)$ of the spectroscopic LRG sample from the SDSS. We have detected positive alignment between pairs of the LRGs up to $\sim 30 h^{-1}$ Mpc scales. More luminous LRGs have a stronger correlation of ellipticity than less luminous ones although the error bars are large, while no significant evidence is found for redshift dependence between redshifts 0.2 and 0.4.

Accurate measurement of spectroscopic redshifts enables us to divide our LRG sample into centrals and satellites. In order to examine the existence of misalignment between central LRGs and their host dark matter halos, we employed a high-resolution N-body simulation. Adopting the best-fit HOD parameters of the LRGs already obtained in previous studies, we assigned central and satellite LRGs to simulated halos. Then we measured the model ellipticity correlation functions from the mock central LRGs. The ellipticity correlation is predicted to have the same shape as, but an amplitude about four times higher than, our observation if the central LRGs are perfectly aligned with their host halos.

We assumed misalignment of the central LRGs with their parent dark halos to follow a Gaussian distribution with zero mean and a width σ_θ. By comparing the observed ellipticity correlation function c_{11} with its model predictions, we have obtained a tight constraint on the misalignment parameter as $\sigma_\theta = 35.4^{+4.0}_{-3.3}$. A model that the LRGs and host halos are completely aligned was strongly rejected in our analysis. This is an accurate detection of the misalignment using observed data.

The results have important implications for weak lensing observations. To be specific for the current discussion, we assume that the source galaxies are at redshift about 1 and have limiting magnitude $R_{AB} = 24.5$ similar to that of a recent large CFHTLS weak lensing survey (Fu et al. 2008). From the HOD analysis by Zheng et al. (2007) for the clustering of galaxies in the DEEP2 redshift survey which has a similar limiting magnitude, we know that more than $\sim 80\%$ of these source galaxies are central galaxies in dark matter halos $\sim 4 \times 10^{11} h^{-1} M_\odot$. If these central galaxies have the same misalignment distribution relative to their host halos as the

LRGs, we expect that the intrinsic ellipticity correlation of the galaxies is about four times smaller than that of the hosting halos. Considering that the distribution of the intrinsic ellipticity of the galaxies at $z \approx 1$ is quite similar to that of host halos (G. Gao et al. 2009, in preparation), we expect that this intrinsic ellipticity correlation of galaxies can contribute by about 5% to the shear correlation according to the ellipticity correlation function of halos (Figure 3 of Jing 2002) and the shear power spectrum (e.g., Wittman et al. 2000; Kaiser 2000). The contribution is decreased if the blue disk galaxies are misaligned more with their host halos than the red ones (see Yang et al. 2006). A more precise assessment of the impact on the weak lensing observations will be discussed in a future paper based on more detailed modeling of galaxies in halos.

The misalignment distribution of the LRGs can also serve as a test for the formation of giant ellipticals. The dry and gas-rich mergers may result in different properties of elliptical galaxies, including their orientations. This may also serve a test for the hierarchical formation scenario of galaxies. We will compare this observation with the central galaxies in a hydro/*N*-body cosmological simulation in a future paper.

The current SDSS-II Legacy Survey will be completed in the next Data Release. However, an upcoming survey, the SDSS-III's Baryon Oscillation Spectroscopic Survey (BOSS)[3], is planned to intensively survey the LRGs at the more distant universe, $0.5 < z < 0.8$. Although the main goal of the BOSS is accurate measurement of cosmological distance scales using baryon acoustic oscillations (e.g., Eisenstein et al. 2005), it will also enable us to discuss the evolutionary effects of LRGs. When LRGs at wider redshift ranges are available, we will be able to improve the results obtained in this work. Then the luminosity and redshift dependences of misalignment between central galaxies and their host halos will be discussed more accurately, which will lead to a better understanding of galaxy formation and evolution.

REFERENCES

Adelman-McCarthy, J., et al. 2008, ApJS, 175, 297
Berlind, A. A., & Weinberg, D. H. 2002, ApJ, 575, 587
Bernstein, G., & Norberg, M. 2002, AJ, 124, 733
Blake, C., Collister, A., & Lahav, O. 2008, MNRAS, 385, 1257
Boylan-Kolchin, M., Ma, C.-P., & Quataert, E. 2006, MNRAS, 369, 1081
Brainerd, T. G. 2005, ApJ, 628, L101
Bridle, S., & King, L. 2007, New J. Phys., 9, 444
Brown, M. L., Taylor, A. N., Hambly, N. C., & Dye, S. 2002, MNRAS, 333, 501
Catelan, P., Kamionkowski, M., & Blandford, R. D. 2001, MNRAS, 320, L7
Chen, D. N., Jing, Y. P., & Yoshikaw, K. 2003, ApJ, 597, 35
Crittenden, R. G., Natarajan, P., Pen, U., & Theuns, T. 2001, ApJ, 559, 552
Croft, R. A. C., & Metzler, C. A. 2000, ApJ, 545, 561
Dubinski, J. 1998, ApJ, 502, 141
Eisenstein, D. J., et al. 2001, AJ, 122, 2267
Eisenstein, D. J., et al. 2005, ApJ, 633, 560
Faltenbacher, A., Li, C., Mao, S., van den Bosch, F. C., Yang, X., Jing, Y. P., Pasquali, A., & Mo, H. J. 2007, ApJ, 662, L71
Fan, Z.-H. 2007, ApJ, 669, 10
Fischer, P., et al. 2000, AJ, 120, 1198
Fu, L., et al. 2008, A&A, 479, 9
Heavens, A., Refregier, A., & Heymans, C. 2000, MNRAS, 319, 649
Heymans, C., Brown, M., Heavens, A., Meisenheimer, K., Taylor, A., & Wolf, C. 2004, MNRAS, 347, 895
Heymans, C., & Heavens, A. 2003, MNRAS, 339, 711
Heymans, C., White, M., Heavens, A., Vale, C., & Waerbeke, L. V. 2006, MNRAS, 371, 750
Hirata, C. M., Mandelbaum, R., Ishak, M., Seljak, U., Nichol, R., Pimbblet, K. A., Ross, N. P., & Wake, D. 2007, MNRAS, 381, 1197
Hirata, C. M., & Seljak, U. 2004, Phys. Rev. D, 70, 063526
Hirata, C. M., et al. 2004, MNRAS, 353, 529
Ho, S., Lin, Y.-T., Spergel, D., & Hirata, C. M. 2007, arXiv:0706.0727
Hoekstra, H., Yee, H. K. C., & Gladders, M. D. 2004, ApJ, 606, 67
Hui, L., & Zhang, J. 2008, ApJ, 688, 742
Jing, Y. P. 2002, MNRAS, 335, L89
Jing, Y. P., Mo, H. J., & Börner, G. 1998, ApJ, 494, 1
Jing, Y. P., & Suto, Y. 2002, ApJ, 574, 538
Jing, Y. P., Suto, Y., & Mo, H. J. 2007, ApJ, 657, 664
Joachimi, B., & Schneider, P. 2008, A&A, 488, 829
Kaiser, N., Wilson, G., & Luppino, G. A. 2000, arXiv:astro-ph/0003338
Kang, X., van den Bosch, F. C., Yang, X., Mao, S., Mo, H. J., Li, C., & Jing, Y. P. 2007, MNRAS, 378, 1531
King, L. J. 2005, A&A, 441, 47
King, L., & Schneider, P. 2002, A&A, 396, 411
Kulkarni, G. V., Nichol, R. C., Sheth, R. K., Seo, H.-J., Eisenstein, D. J., & Gray, A. 2007, MNRAS, 378, 1196
Lee, J., & Pen, U. L. 2000, ApJ, 532, L5
Lee, J., & Pen, U. L. 2001, ApJ, 555, 106
Lee, J., & Pen, U. L. 2007, ApJ, 670, L1
Lee, J., & Pen, U. L. 2008, ApJ, 681, 798
Lupton, R. H 1993, Statistics in Theory and Practice (Princeton, NJ: Princeton Univ. Press)
Lupton, R. H., Gunn, J. E., Ivezic, Z., Knapp, G. R., Kent, S., & Yasuda, N. 2001, in ASP Conf. Ser. 238, Astronomical Data Analysis Software and Systems X, ed. F. R. Jr. Harnden, F. A. Primini, & H. E. Payne (San Francisco, CA: ASP) 269 (arXiv:astro-ph/0101420)
Ma, C.-P., & Fry, J. N. 2000, ApJ, 543, 503
Mandelbaum, R., Hirata, C. M., Broderick, T., Seljak, U., & Brinkmann, J. 2006a, MNRAS, 370, 1008
Mandelbaum, R., Hirata, C. M., Ishak, M., Seljak, U., & Brinkmann, J. 2006b, MNRAS, 367, 611
Mandelbaum, R., et al. 2005, MNRAS, 361, 1287

---

[3] http://www.sdss3.org/cosmology.php.

Masjedi, M., et al. 2006, ApJ, 644, 54
Miralda Escudé, J. 1991, ApJ, 380, 1
Naab, T., Khochfar, S., & Burkert, A. 2006, ApJ, 636, L81
Navarro, J. F., Frenk, C. S., & White, S. D. M. 1997, ApJ, 490, 493
Peacock, J. A., & Smith, R. E. 2000, MNRAS, 318, 1144
Pen, U. L., Lee, J., & Seljak, U. 2000, ApJ, 543, L107
Percival, W. J., et al. 2007, ApJ, 657, 645
Reid, B. A., & Spergel, D. N. 2008, arXiv:0809.4505
Schlegel, D. J., Finkbeiner, D. P., & Davis, M. 1998, ApJ, 500, 525
Scoccimarro, R., Sheth, R. K., Hui, L., & Jain, B. 2001, ApJ, 546, 20
Seljak, U. 2000, MNRAS, 318, 203
Seo, H.-J., Eisenstein, D. J., & Zehavi, I. 2008, ApJ, 681, 998
Sharma, S., & Steinmetz, M. 2005, ApJ, 628, 21
Stoughton, C., et al. 2002, AJ, 123, 485
Takada, M., & White, M. 2004, ApJ, 601, L1

van den Bosch, F. C., Abel, T., Croft, R. A. C., Hernquist, L., & White, S. D. M. 2002, ApJ, 576, 21
Wang, Y., Yang, X., Mo, H. J., Li, C., van den Bosch, F. C., Fan, Z., & Chen, X. 2008, MNRAS, 385, 1511
White, M., Zheng, Z., Brown, M. J. I., Dey, A., & Jannuzi, B. T. 2007, ApJ, 655, L69
Wittman, D. M., Tyson, J. A., Dell'Antonio, I., & Bernstein, G. 2000, Nature, 405, 143
Yang, X., van den Bosch, F. C., Mo, H. J., Mao, S., Kang, X., Weinmann, S. M., Guo, Y., & Jing, Y. P. 2006, MNRAS, 369, 1293
York, D. G., et al. 2000, AJ, 120, 1579
Zehavi, I., et al. 2005, ApJ, 621, 22
Zheng, Z., Coil, A. L., & Zehavi, I. 2007, ApJ, 667, 760
Zheng, Z., Zehavi, I., Eisenstein, D. J., Weinberg, D. H., & Jing, Y. P. 2008, arXiv:0809.1868
Zheng, Z., et al. 2005, ApJ, 633, 791